AIAA AVIATION Forum
August 2-6, 2021, VIRTUAL EVENT
AIAA AVIATION 2021 FORUM

10.2514/6.2021-2585

Numerical Investigation of Co-Flow Jet 3D Transonic Wings

Jeremy Boling*,Ge-Cheng Zha†
Department of Mechanical and Aerospace Engineering
University of Miami, Coral Gables, Florida 33124
E-mail: gzha@miami.edu

This paper numerically investigates CoFlow Jet (CFJ) 3D transonic wings formed with the 10% thickness NASA SC(2)-1010 and the 12% thickness RAE-2822 airfoils. The present research is based on validated CFD simulation, which employs 3D RANS solver with Spalart-Allmaras (S-A) turbulence model, 3rd order WENO scheme for the inviscid fluxes, and 2nd order central differencing for the viscous terms. For zero sweep and aspect ratio of 10, the CFJ-NASA SC(2)-1010 wing is shown to increase cruise-efficiency C_L/C_{Dc} by 10% and lift coefficient by 10% simultaneously over the baseline wing. When the sweep angle is increased to 10°, the improvement is decreased. Similarly, wings formed by CFJ-RAE-2822 are able to increase aerodynamic efficiency at zero sweep and aspect ratio of 10. Decreasing the CFJ jet strength from root to tip is beneficial to reduce drag and power consumption while maintaining lift enhancement due to decreased tip loading. Applying the CoFlow Jet to only the inner span of the CFJ-RAE-2822 wing sees a CFJ power reduction benefit over having injection and suction extend to the wing tip. This method also provides a lift and cruise efficiency benefit over the baseline wing. The outer 30% span shows a diminished supersonic region. Applying the CFJ to the innjer 70% results in reduced power consumption while increasing performance including a 1.2% increase in aerodynamic efficiency over baseline and a 5.7% improvement in lift coefficient in case CFJ-3D-14. Productivity efficiency is similarly increased by 7.1%.

Nomenclature

V	Flow Velocity
ρ	Air Density
α, AoA	Angle of Attack
$\dot{m}$	Mass Flow Rate
M	Mach Number
M_i	Isentropic Mach Number
Re	Reynolds Number
L	Aerodynamics Lift
D	Aerodynamic Drag
p	Static Pressure
p_0	Total Pressure
η	Pumping Power
q_∞	Freestream Dynamic Head, $\frac{1}{2}\rho_\infty {V_\infty}^2$
C_L	Lift Coefficient, $\frac{L}{q_\infty S}$
C_{LMAX}	Maximum Lift Coefficient
C_D	Drag Coefficient, $\frac{D}{q_\infty S}$
C_M	Moment Coefficient, $\frac{M}{q_\infty S c}$
C_{M_α}	Slope of Moment Coefficient vs Angle of Attack
C_p	Pressure Coefficient, $\frac{p-p_\infty}{q_\infty}$

*PhD Candidate
†Professor, AIAA Associate Fellow

C_μ	Jet Momentum Coefficient, $\frac{\dot{m}_j v_j}{q_\infty S}$
$(\frac{L}{D})$	Conventional Aerodynamic Efficiency
P_c	Power Coefficient, $\frac{L}{q_\infty S V_\infty}$
$(\frac{L}{D})_c$	Corrected Aerodynamic Efficiency for CFJ Airfoil, $\frac{L}{D+P/V_\infty} = \frac{C_L}{C_D+P_c}$
$(\frac{C_L^2}{C_D})$	Productivity Efficiency Coefficient
$(\frac{C_L^2}{C_D})_c$	Corrected Productivity Efficiency Coefficient for CFJ Airfoil
∞	Free Stream Conditions

I. Introduction

I.A. 3D Transonic Wings

Airfoils determine the basic aerodynamic performance of a wing, and the wing with a finite span formed by the airfoil determines aircraft performance. For a finite wing, the flow around the wing tips builds into a circular motion that forms the wingtip vortex, and represents lost energy. Not only does the wing bleed off energy with tip vortices, it also generates downwash that reduces the angle of attack of the wing and creates induced drag. For a sufficiently long wing span with a high aspect ratio, the energy loss or drag increase due to tip vortex will be small. When the flow speed approaches high subsonic such as 0.6 or above, the transonic flow wave drag is significant. Adding a sweep angle to a transonic wing is the typical way to increase the critical Mach number and reduces wave drag. Liu and Zha[1] apply the coflow jet (CFJ) active flow control for the 2D RAE2822 airfoil and are able to significantly increase the cruise lift coefficient and aerodynamic efficiency at the same time. Boling et al[2] investigate the low speed performance of 2D transonic supercritical airfoil using CFJ AFC. Their results indicate that the 2D supercritical airfoil is able to achieve very high lift coefficient at low speed without using flaps due to the CFJ enhancement. So far, no study on coflow jet application to 2D transonic supercritical wings is done. The purpose of this paper is to investigate the issues that need to be addressed in how the CoFlow jet will enhance the 3D wing performance at transonic Mach numbers, including the effects of aspect ratio and wing sweep.

I.B. CFJ Active Flow Control

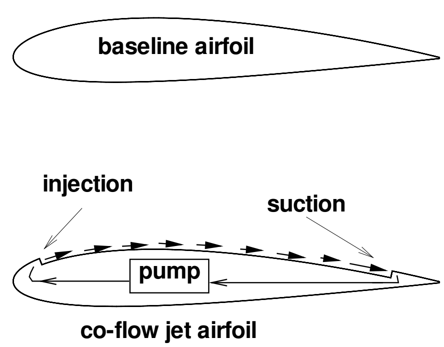

Figure 1: The CFJ airfoil control volume schematic.

The Co-Flow Jet airfoil is a zero-net mass-flux(ZNMF) active flow control technique developed by Zha et al.[1,3–15] Using this technique applied to a traditional airfoil provides the ability to increase lift and aerodynamic efficiency at low energy expenditure. This low energy expenditure results from placing an injection slot near the leading edge and a suction slot near the trailing edge as shown in Fig. 1. A small amount of mass flow is injected near the leading edge, tangential to the airfoil suction surface and sucked in at a position of higher pressure near the trailing edge. Applied to an airfoil, these locations resemble Figure 1.

This technique works by energizing the boundary layer and hence increasing circulation, augmenting lift while decreasing pressure drag due to enhanced leading edge suction and filled wake.

II. Methodology

II.A. CFJ Airfoil Parameters

II.A.1. Drag and Lift

Zha et al.[5] give the following formulations to calculate the lift and drag due to CFJ effect for CFD simulation

$$R_x = (\dot{m}_j V_{j1} + p_{j1} A_{j1})\ cos(\theta_1 - \alpha) - (\dot{m}_j V_{j2} + p_{j2} A_{j2})\ cos(\theta_2 + \alpha) \tag{1}$$

$$R_y = (\dot{m}_{j1} V_{j1} + p_{j1} A_{j1})\ sin(\theta_1 - \alpha) + (\dot{m}_{j2} V_{j2} + p_{j2} A_{j2})\ sin(\theta_2 + \alpha) \tag{2}$$

where x and y represent the drag and lift direction respectively, subscripts 1 and 2 stand for the injection and suction, θ_i $(i = 1, 2)$ is the angle between the injection or suction slot surface and the line normal to the airfoil chord, and α is the AoA, as shown in Figure 2.

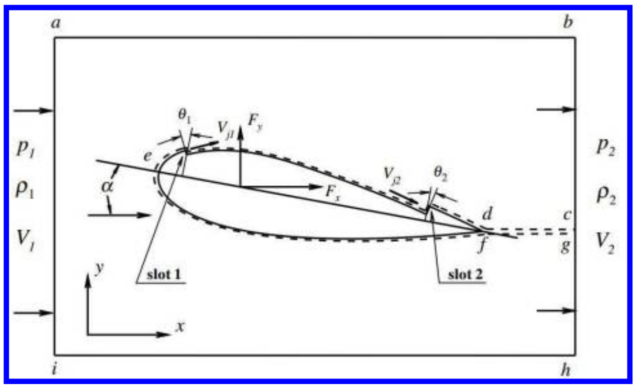

Figure 2: The CFJ airfoil control volume schematic.

The total drag and lift of the CFJ airfoil can then be expressed as below

$$D = F_x - R_x \tag{3}$$

$$L = F_y - R_y \tag{4}$$

where F_x and F_y are the drag and lift force due to surface integral of pressure and shear stress. The corresponding drag and lift coefficients are expressed as following

$$C_D = \frac{D}{\frac{1}{2}\rho_\infty {V_\infty}^2 S} \tag{5}$$

$$C_L = \frac{L}{\frac{1}{2}\rho_\infty {V_\infty}^2 S} \tag{6}$$

where ρ_∞ and V_∞ denote the free stream density and velocity. S is the wing planform area. For 2-D airfoil study, S denotes the planform area per unit span, which is equal to the airfoil chord length.

II.A.2. Jet Momentum

The jet momentum coefficient C_μ is a parameter used to quantify the jet intensity, which is defined as

$$C_\mu = \frac{\dot{m} V_j}{\frac{1}{2}\rho_\infty {V_\infty}^2 S} \tag{7}$$

where $\dot{m}$ is the injection mass flow rate, V_j is the averaged injection velocity at the injection slot opening.

II.A.3. Power Consumption

The CFJ can be implemented by mounting a pumping system inside the wing that withdraws air from the suction slot and blows it into the injection slot. The power consumption can be determined by the jet mass flow and total enthalpy change as follows

$$P = \dot{m}(H_{01} - H_{02}) \tag{8}$$

where H_{01} and H_{02} are the total enthalpy in the injection cavity and suction cavity, respectively. P is the power required by the pump. Introducing the pump efficiency η and total pressure ratio of the pump $\Gamma = \frac{P_{01}}{P_{02}}$, the power consumption can be expressed as

$$P = \frac{\dot{m} C_p T_{02}}{\eta}(\Gamma^{\frac{\gamma-1}{\gamma}} - 1) \tag{9}$$

where γ is the specific heat ratio for air. The power consumption can be further normalized as a power coefficient

$$P_c = \frac{P}{\frac{1}{2}\rho_\infty V_\infty^3 S} \tag{10}$$

II.A.4. Aerodynamic Efficiency

The conventional airfoil aerodynamic efficiency is defined as

$$(\frac{L}{D}) = \frac{C_L}{C_D} \tag{11}$$

For the CFJ airfoil, the ratio above represents the pure aerodynamic relationship between lift and drag. Taking into account the energy consumption of the CFJ, the conventional aerodynamic efficiency is modified by converting the power consumption into a corresponding drag force. The equation of the corrected aerodynamic efficiency is given as follows[10]

$$(\frac{L}{D})_c = \frac{L}{D + \frac{P}{V_\infty}} \tag{12}$$

in which the pump power consumption P is converted into a force $\frac{P}{V_\infty}$ added to the aerodynamic drag D. The formulation above can be further expressed using the non-dimensional coefficients C_L, C_D and P_c as

$$(\frac{L}{D})_c = \frac{C_L}{C_D + P_c} \tag{13}$$

Note that when the pumping power is set to 0, $(\frac{L}{D})_c$ returns to conventional aerodynamic efficiency definition.

A productivity efficiency parameter was introduced by Yang et al.[14] It describes the capability to transport a gross weight for maximum distance at cruise.

$$(\frac{C_L^2}{C_D})_c = \frac{C_L^2}{C_D + P_c} \tag{14}$$

The transonic airfoils NASA SC(2)-1010 and RAE 2822 are used to form the 3D wings studied. They represent airfoil thickness of 10% and 12% respectively. Suction surface translation (SST) is maintained at 0.05% from previous studies.[1]

The suction slot size, orientation and location are also maintained based on the best performing results at cruise conditions from the 2D study in a previous study.[1,2] The injection slot is placed at 4% chord location for NASA SC(2)-1010 and 3% chord location for RAE-2822 3D wings. Free-stream values for cruise conditions are $M = 0.701$ and $Re = 6 \times 10^6$, based on validation of the NASA SC(2)-1010. The cruise condition for RAE-2822 is M=0.729 and $Re = 6.5 \times 10^6$, based on the validation efforts of Liu.[1]

II.B. Numerical Approach

The in house FASIP (Flow-Acoustics-Structure Interaction Package) CFD code is used to conduct the numerical simulation. A 3rd order WENO scheme for the inviscid flux and a 2nd order central differencing for the viscous terms are employed to discretize the Navier-Stokes equations. The low diffusion E-CUSP scheme used as the approximate Riemann solver suggested by Zha et al[16] is utilized with the WENO scheme to evaluate the inviscid fluxes. Implicit time marching method using Gauss-Seidel line relaxation is used to achieve a fast convergence rate. Parallel computing is implemented to save wall clock simulation time.[17]

II.C. Boundary Conditions

The 3rd order accuracy no slip condition is enforced on the solid surface with the wall treatment suggested in Shen et al.[18] to achieve the flux conservation on the wall. Total pressure, total temperature and flow angles are specified at the injection duct inlet, as well as the upstream portion of the far field. For the static condition, the static pressure at the downstream farfield is set to be equal to the total pressure at upstream far field. Constant static pressure is applied at the suction duct outlet as well as the downstream portion of the far field. The first grid point on the wing surface is placed at $y+ = 1$.

II.D. Computational Mesh

The two-dimensional NASA SC(2)-1010 airfoil is stacked into a three-dimensional wing. The mesh for the airfoil section is based on the validated 2D results. It is based on the more refined 601×151 mesh size. The domain size is altered for 3D to $521 \times 81 \times 121$ around the airfoil, in the radial direction, and in the spanwise direction. The far field is chosen to be a zero-gradient boundary condition, and the wing root is chosen to have a symmetry boundary condition. The radial far-field is maintained at 20 chord lengths, while the far-field away from the wing-tip is also specified to be 20 chord lengths in order to properly capture the three-dimensional effects of the flow. An example of the mesh topology for a wing with an aspect ratio of 10 can be seen in Figure 3. The mesh contains 5.4 million cells split into 47 blocks for parallel computation. The first grid point on the wing surface is located at $y^+ = 1$. The mesh is refined near the wing tip in order to resolve the wingtip vortex.

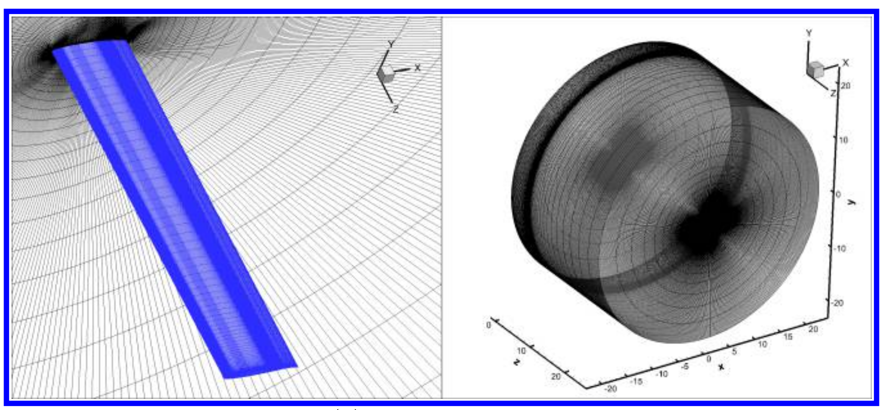

Figure 3: NASA SC(2)-1010 3D wing, aspect ratio 10 mesh

The 3D CFJ study of a finite wing with NASA SC(2)-1010 airfoil is created with aspect ratio of 10. The injection slot is maintained at 4% along the chord, with the injection slot at 75% of the chord. The CFJ slots are formed from the root to the tip. The tip has a wall boundary condition where the slots end. The injection and suction slots contain 512,000 total cells. The upper and lower surfaces of the injection suction slots use wall boundary conditions.

The 3D RAE-2822 wing mesh is constructed with an O-mesh topology for high quality all the way around the wing. The total number of cells is 5.4 million split into 84 blocks for parallel computation. It is based on the 2D airfoil mesh from the previous study. The mesh measures 521 cells around the wing, 121 cells in the spanwise direction, and 81 cells in the radial direction. The far-field extends 20 chord lengths radially and 20 chord lengths in the span-wise direction beyond the tip. The mesh is refined near the tip to resolve wingtip vortices and span-wise flow.

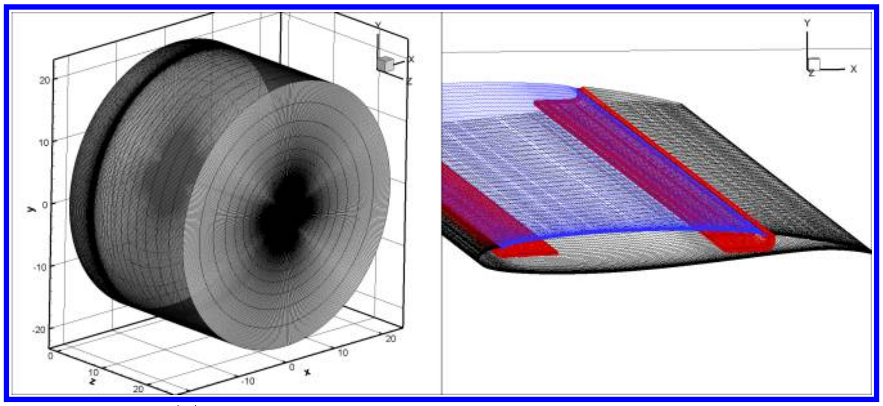

Figure 4: NASA SC(2)-1010 3D wing, aspect ratio 10 computational mesh and injection and suction slots

The CFJ-RAE-2822 mesh shares the same topology and domain size as the baseline mesh with a few added blocks for the CFJ slot. The total cell count is 6.6 million split into 100 blocks. The larger mesh size is due to the SST having its own set of blocks. Similarly, the first cell location in the SST mesh is at $y^+ = 1$. The Injection and suction slots are inside the wing and can be seen in Figure 5. They are unchanged from the 2D airfoil mesh.

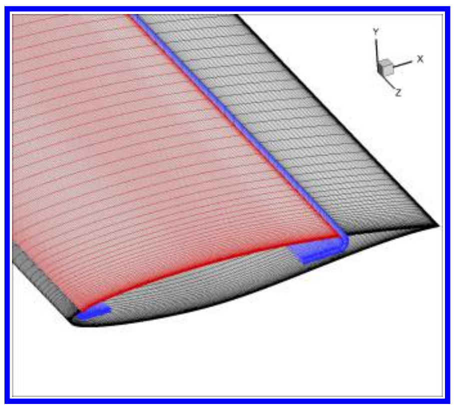

Figure 5: CFJ-RAE-2822 AR10 3D mesh

III. Results and Discussions

III.A. Baseline Wing with NASA SC(2)-1010 Airfoil with AR of 10

The wing stacked by the baseline NASA SC(2)-1010 airfoil with no sweep at aspect ratio of 5, 10, 15, and 20 respectively are studied for comparison. Figure 6 shows the Mach number contours and streamlines for the wing with aspect ratio of 10. The Mach number contours show a higher Mach number at the root of the wing and decreasing Mach number toward the wing tip due to three-dimensional tip vortex effects. The wing is not tapered. The curved streamlines at the tip indicate the three-dimensional wing effects and wingtip vortex, which reduces the aerodynamic efficiency compared with 2D airfoil. The flow with higher Mach number near the root of the wing more closely resembles the 2D flow.

Fig. 7 shows the C_L vs AoA, drag polar, and C_L/C_D vs AoA against angle of attack. With the increase of the aspect ratio, the lift coefficient and C_L/C_D are increased due to the reduced 3D effect. The study indicates that the optimum aerodynamic efficiency occurs at AoA of $-2°$.

Figure 8 shows the isentropic Mach number distribution at the root and mid-span of the baseline wing of aspect ratio 10 and AoA of $0°$ compared with the 2D airfoil result. Although the flow accelerates to the same local velocity as the 2D baseline case at the leading edge, the 3D Mach number drops off more quickly. The suction peak is in the same location, which may benefit the CFJ wing based on the same 2D configuration. The 3D shock wave is a little weaker than the 2D result and the shock location is also more upstream.

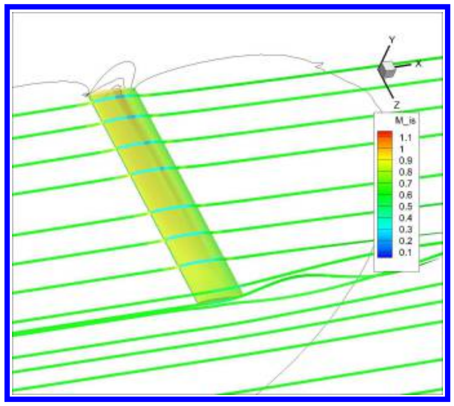

Figure 6: NASA SC(2)-1010 3D baseline wing, Isentropic Mach surface contours, aspect ratio 10 with streamlines

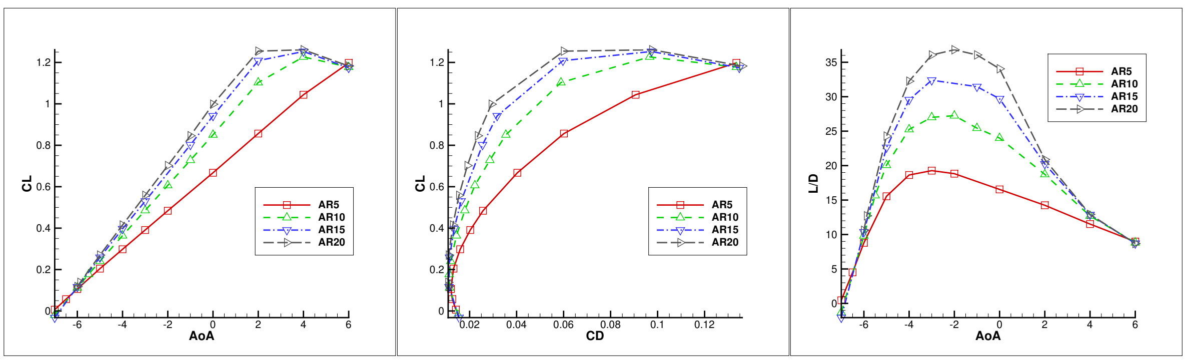

Figure 7: Baseline 3D wing with NASA SC(2)-1010 airfoil, 0 degree sweep, AR=5, 10, 15, 20

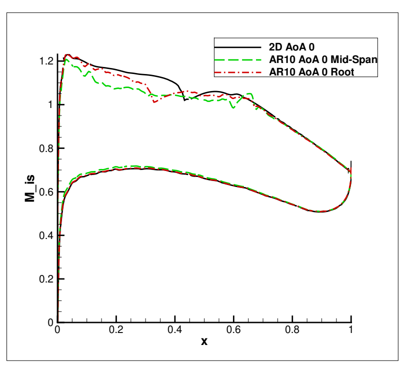

Figure 8: Baseline 3D wing with NASA SC(2)-1010 airfoil isentropic Mach distribution at root and mid-span

III.B. NASA SC(2)-1010 CFJ Wing with AR of 10

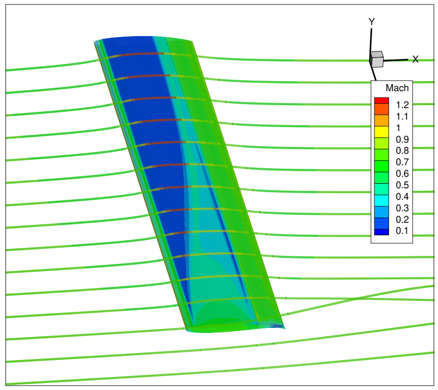

Figure 9: Surface pressure contours of the 3D wing with CFJ-NASA SC(2)-1010 airfoil, aspect ratio 10 with streamlines colored by Mach number

Figure 9 is representative of the first part of the CFJ wing sweep study at C_μ of 0.004 and zero sweep. The 3D streamlines are colored by Mach numbers, while the surface contours of the wing are the local static pressure. The pressure contours clearly show the normal shock position varying from the root to near leading edge at the wing tip. Near the root the supersonic region occupied almost half of the chord like the 2D airfoil, while at the tip the flow is supersonic near the suction peak and quickly decelerates. This near tip region does not appear to be as effective as in the inner span for the CFJ since the CFJ acts mostly downstream of the normal shock.

Fig. 10 shows several parameters varying with the AoA at constant C_μ of 0.004, including (a) lift coefficient C_L, (c) corrected aerodynamic efficiency $(C_L/C_D)_c$, (d) productivity efficiency $(C_L^2/C_D)_c$, (e) CFJ power coefficient Pc, (f) CFJ total pressure ratio PR, (f) ratio of injection velocity to freestream velocity, (h) normalized mass flow rate, and the drag polar in (b). The lift coefficient of the CFJ wing is consistently higher than that of the baseline wing. The drag coefficients are smaller as shown in the drag polar (b). This is consistent with the previous 2D result. These improvements in lift and drag, along with the typical low power coefficient, contribute to an increase in corrected lift-to-drag ratio and productivity efficiency as shown in Fig. 10 [(c) and (d)]. Table 1 compares the baseline wing and the CFJ wing with AR of 10 at AoA of 0° and 3°, which are the peak productivity and aerodynamic efficiency AoA respectively for the baseline wing.

Table 1: NASA SC(2)-1010 0° sweep, M=0.701, AR=10

Type	α	C_μ	C_L	C_D	P_C	PR	V_{inj}	m_{inj}	$(\frac{L}{D})$	$(\frac{L}{D})_c$	$(\frac{C_L^2}{C_D})_c$
Baseline	0	0	0.8535	0.0350	0	-	-	-	24.43	24.43	20.85
Baseline	-3	0	0.4869	0.0178	0	-	-	-	27.40	27.40	13.34
CFJ	0	0.004	0.9373	0.0347	0.00123	1.104	0.583	0.171	26.97	26.13	24.49
CFJ	-3	0.004	0.5222	0.0161	0.00137	1.143	0.524	0.174	32.48	29.92	15.63

Table 2: NASA SC(2)-1010 0° sweep, M=0.701

Type	α	C_μ	C_Dp	C_Dv	C_Lp	C_Lv	R_x	R_y	C_M
Baseline	-3	-	0.0116	0.00614	0.4868	9.53E-5	-	-	-0.1879
CFJ	-3	0.004	0.0165	0.00582	0.5741	-1.72E-5	0.00632	0.0519	-0.1954

Table 1 clearly indicates an improvement in corrected lift-drag ratio by nearly 10%. This improvement at $\alpha = -3°$ comes from an improved lift coefficient, reduced drag, and a low power consumption. At AoA of 0°, the CFJ wing has the productivity efficiency improved by 17.5% and the lift coefficient increased by 9.8%.

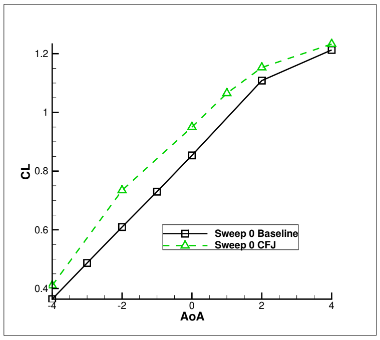

(a) C_L vs. AoA

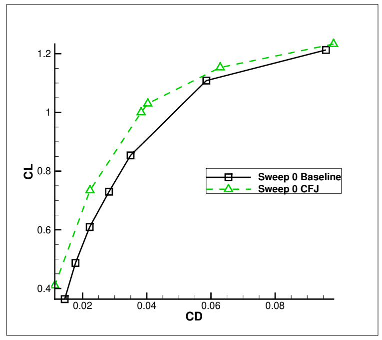

(b) C_L vs. C_D

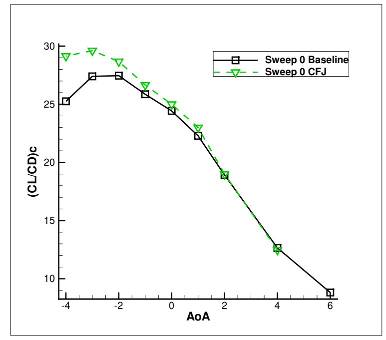

(c) $(C_L/C_D)_c$ vs. AoA

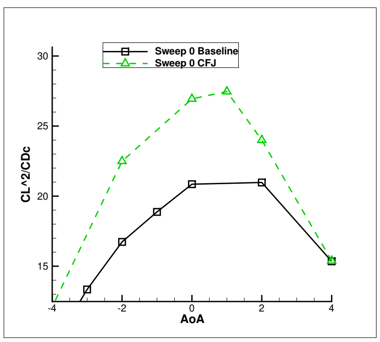

(d) $(C_L^2/C_D)_c$ vs. AoA

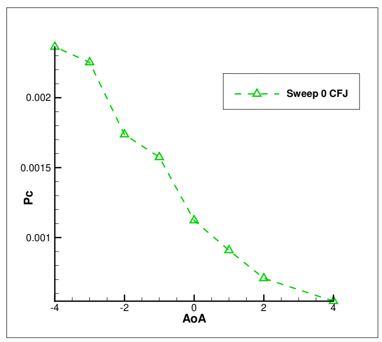

(e) P_c vs. AoA

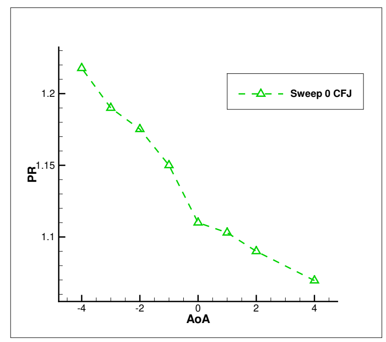

(f) Total pressure ratio vs. AoA

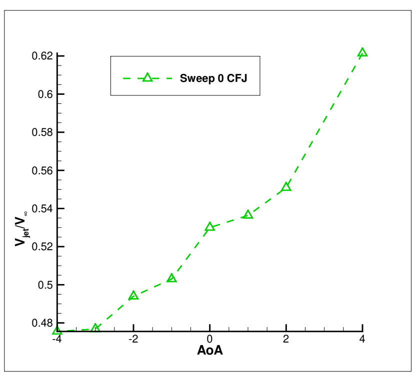

(g) Jet velocity vs. AoA

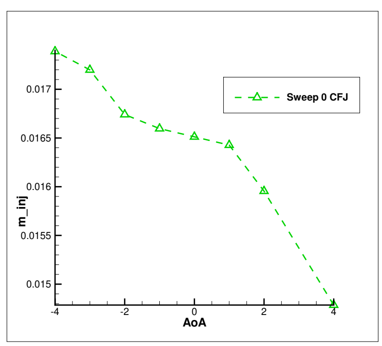

(h) Injection mass flow-rate vs. AoA

Figure 10: Results of the 3D wing with baseline NASA SC(2)-1010 airfoil and CFJ airfoil,, $Cmu = 0.004$, $AR = 10$, $M = 0.701$

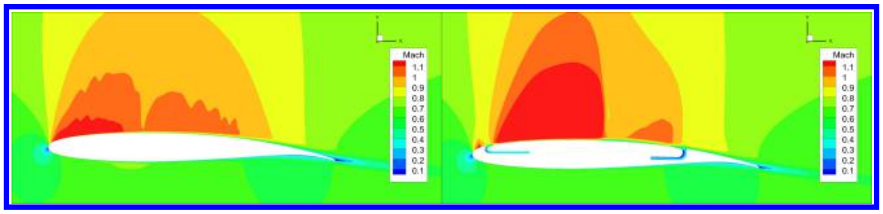

(a) Baseline vs CFJ, Root

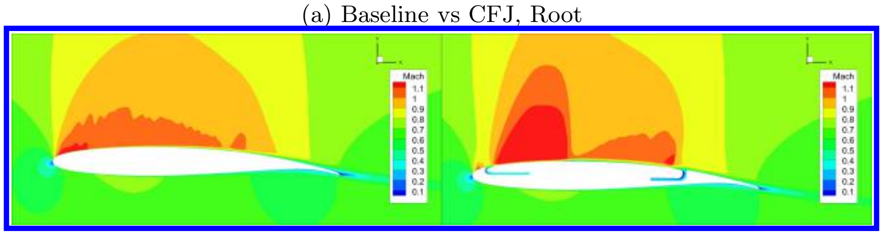

(b) Baseline vs CFJ, Mid-Span

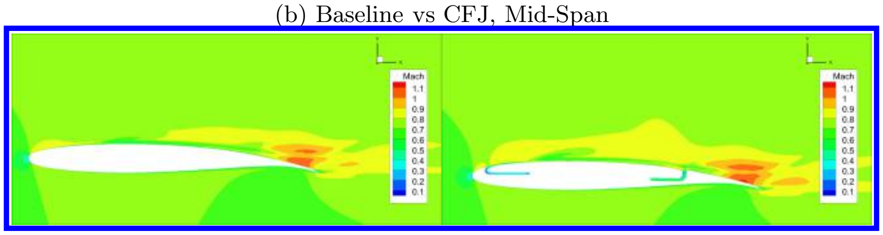

(c) Baseline vs CFJ, Tip

Figure 11: Comparison of NASA SC(2)-1010 Mach contours for the baseline wing (left) and CFJ wing (right), no sweep, $\alpha = 0°$, $C_\mu = 0.004$, $AR = 10$, $M = 0.701$

Figure 11 shows a comparison of the Mach contours of the baseline wing (left) and the CFJ wing (right). The contours represent the sections at the root, mid-span, and wing-tip, respectively. The overall Mach number along the suction surface of the CFJ wing is higher than that of the baseline wing, which generates higher lift coefficient. This effect decreases from root to tip, where the CFJ wing loading is similar to that of the baseline wing since the CFJ does not have much effect at the tip. Reducing the momentum coefficient of the jet results in worse performance and an increase in drag coefficient.

The strengthened supersonic region is seen in more detailed using the isentropic Mach distribution in Figure 12. At 40% span, a shock is formed at about 40% chord location and another shock is formed downstream, just upstream of the suction slot. The entire supersonic region is expanded with higher Mach number than that of the baseline. Table 2 is the breakdown of lift and drag contributions of pressure, surface friction and CFJ reactionary force. Table 2 indicates that the wave drag C_{D_P} of the CFJ is increased, consistent with the stronger shock wave seen in isentropic Mach number distribution (Fig. 12) and the Mach contours(Fig. 11). The jet-reactionary force generates a small thrust, which offsets the wave drag increase of the CFJ wing and results in an overall slightly lower total drag based on Eq. (3). The power coefficients shown in Table 1 are very small, thus increasing the cruise aerodynamic efficiency $(C_L/C_D)c$ by about 10% and productivity efficiency $(C_L^2/C_D)c$ by 17.5%. This study indicates that the 3D transonic wing formed by NASA SC(2) 1010 airfoil with no sweep significantly benefits from the CFJ active flow control as the 2D CFJ airfoil. .

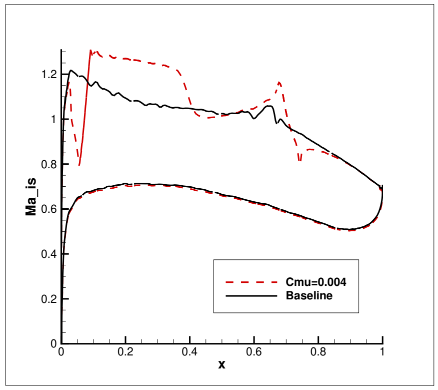

Figure 12: Isentropic Mach distribution at 40% span of the 3D wing with CFJ-NASA SC(2)-1010 airfoil, AR=10, sweep 0°.

III.C. NASA SC(2)-1010 CFJ Wing Sweep Study

III.C.1. 10° Sweep Study

Fig. 13 shows the results of the 10° wing with the same aspect ratio of 10, which shows several parameters varying with the AoA at constant C_μ of 0.004, including (a) lift coefficient C_L, (c) corrected aerodynamic efficiency $(C_L/C_D)_c$, (d) productivity efficiency $(C_L^2/C_D)_c$, (e) CFJ power coefficient Pc, (f) CFJ total pressure ratio PR, (f) ratio of injection velocity to freestream velocity, (h) normalized mass flow rate, and the drag polar in (b). The overall trend of the swept CFJ wing improvement is similar to that of the unswept CFJ wing, but with smaller amount. This could be because that the jet is not fully aligned with the main flow due to the reflection at the turning of the CFJ duct as observed by Xu and Zha.[19]

Figure 14 shows the isentropic Mach number surface contours for the CFJ wing at an AoA of −2°. This is the highest angle of attack that is more aerodynamically efficient than the baseline case. It also maintains a supersonic region above the suction surface.

Figure 15 shows a top-down view of the wing with surface isentropic Mach number contours and streamlines colored by total pressure. The streamlines of the CFJ injection are normal to the leading edge of the wing. The surface isentropic Mach number contours indicates increased loading at mid-span. Figure 16 compares the isentropic Mach number distribution at the root and mid-span. The CFJ wing with 10° sweep angle shows higher loading at mid-span than at the root. The wing with no sweep does not display this behavior in Fig 16.

Table 3: NASA SC(2)-1010 10° Sweep, M=0.712.

Type	α	C_μ	C_L	C_D	P_C	$(\frac{L}{D})_c$	$(\frac{C_L^2}{C_D})_c$
Baseline	0°	0	0.8442	0.0342	0	24.680	20.832
Baseline	−2°	0	0.5761	0.0211	0	27.305	15.731
Baseline	−3°	0	0.4733	0.0173	0	27.365	12.953
CFJ	0°	0.004	0.8594	0.0339	0.002	23.912	20.550
CFJ	−2°	0.004	0.6139	0.0198	0.0023	27.736	17.027
CFJ	−3°	0.004	0.5144	0.00157	0.0024	28.414	14.616
CFJ	−3°	0.002	0.4844	0.0159	0.0007	29.032	14.063

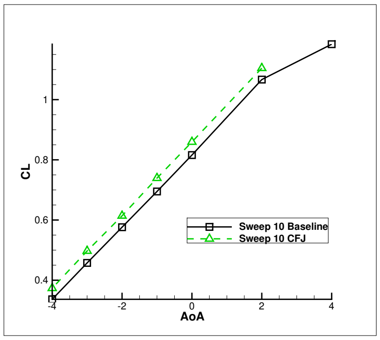

(a) C_L vs. AoA

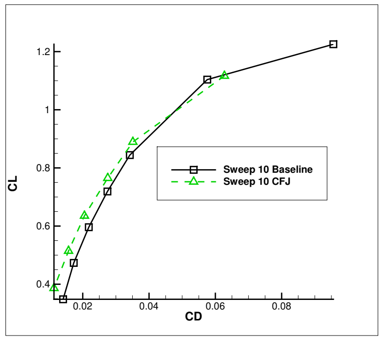

(b) C_L vs. C_D

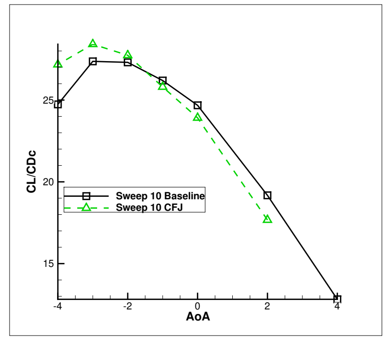

(c) $(C_L/C_D)_c$ vs. AoA

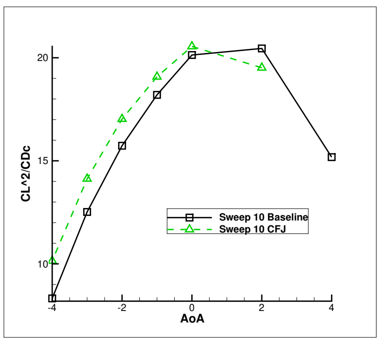

(d) $(C_L^2/C_D)_c$ vs. AoA

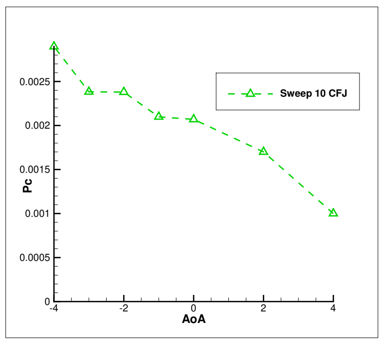

(e) P_c vs. AoA

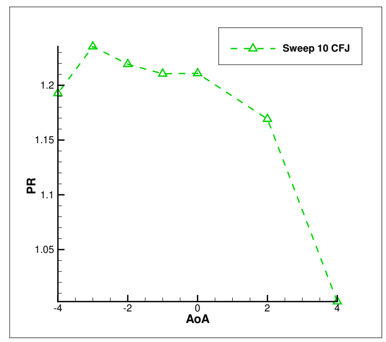

(f) Total pressure ratio vs. AoA

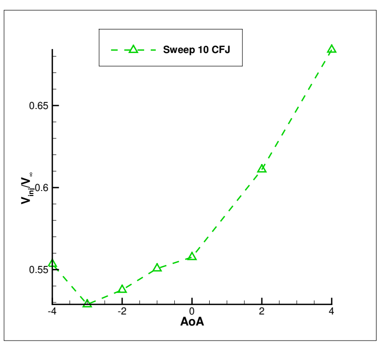

(g) Jet velocity vs. AoA

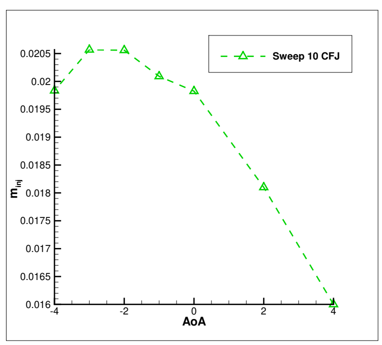

(h) Injection mass flow-rate vs. AoA

Figure 13: NASA SC(2)-1010 baseline v CFJ, 10° sweep, $C_\mu = 0.004$, $AR = 10$, $M = 0.712$

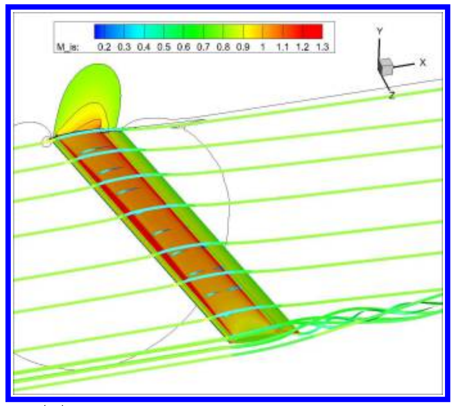

Figure 14: CFJ-NASA SC(2)-1010 wing isentropic Mach surface contours, 10° sweep, $C_\mu = 0.004$, $AR = 10$, $M = 0.712$, $\alpha = -2°$

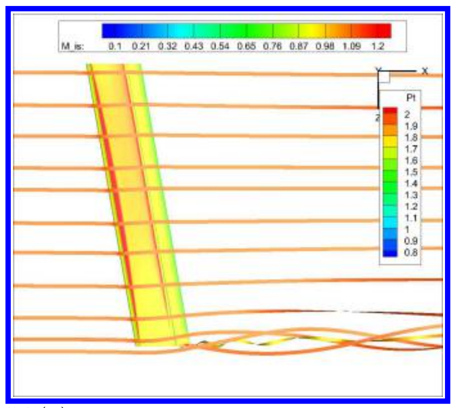

Figure 15: CFJ-NASA SC(2)-1010 wing streamlines with total pressure contours, 10° sweep, $C_\mu = 0.004$, $AR = 10$, $M = 0.712$, $\alpha = -2°$

Table 4: NASA SC(2)-1010 10° Sweep, M=0.712

Type	α	C_μ	C_Dp	C_Dv	C_Lp	C_Lv	R_x	R_y	C_M
Baseline	$-3°$	-	0.0112	0.00613	0.4732	9.562E-5	-	-	-0.1089
CFJ	$-3°$	0.004	0.0164	0.00591	0.5661	2.20E-5	0.00658	0.0517	-0.1311
CFJ	$-3°$	0.002	0.0157	0.00565	0.5348	3.16E-5	0.00541	0.0504	-0.1303

Using the CFJ parameters from the study with no sweep, the CoFlow-Jet wing shows an overall performance improvement over the baseline swept wing as shown in Table 3. The lift coefficient is increased, along with a slight reduction in drag. The pressure drag is higher, as indicated in Table 4, but the jet reactionary force slightly offset the pressure drag. Pressure drag increase is due to a stronger shock, which can be reduced by decreasing C_μ, as shown at $\alpha = -3°$ in Table 3. The corrected lift-to-drag ratio is increased from 27.31 to 27.74 at AoA $-2°$. The peak $(C_L/C_D)_c$ is at AoA $-3°$ with a value of 29.03. This results in an increase of 6% aerodynamic efficiency. This is only achieved after reducing the C_μ from 0.004 to 0.002, showing that a reduction in C_μ can result in decreased pressure drag for this configuration.

Figure 17 shows the Mach contours comparison for the baseline wing and CFJ wing at $\alpha = -3°$ and $C_\mu = 0.002$. At the root, mid-span, and the tip, the Mach number on the CFJ wing suction surface is increased. When looking at the Mach number distribution, it is clear that the flow over the baseline airfoil is in the high subsonic and sonic region. At the root there is slightly supersonic flow with more aft load. At mid-span, the region of high-speed flow is more uniform over the length of the wing. The CFJ wing increases the flow velocity and makes the flow supersonic near the suction slot with a very mild isentropic shock wave. This also means introducing a shock wave. The results indicate that the efficiency increase for the CFJ wing at α of 3° is because the flow is at low supersonic and the shock wave is mostly isentropic.

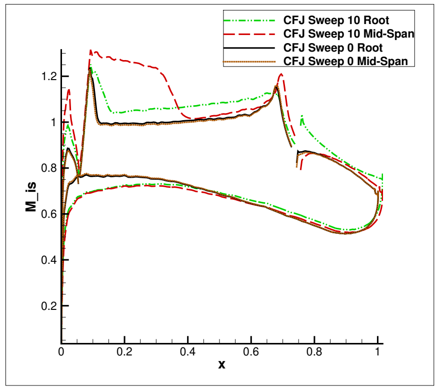

Figure 16: CFJ-NASA SC(2)-1010 Isentropic Mach Number Distribution for ,0° and 10° Sweep, $C_\mu = 0.004$, $AR = 10$, $\alpha = 0°$

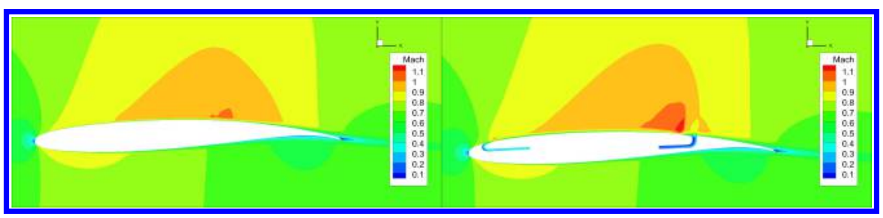

(a) Baseline vs CFJ, Root

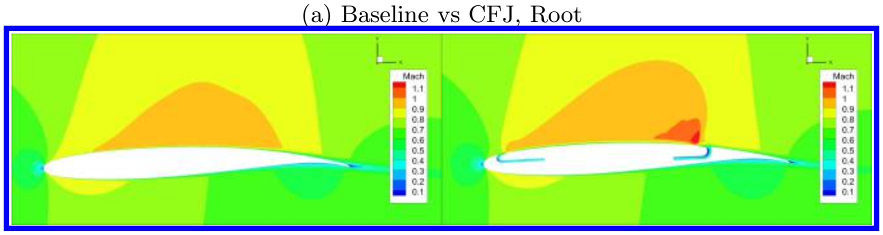

(b) Baseline vs CFJ, Mid-Span

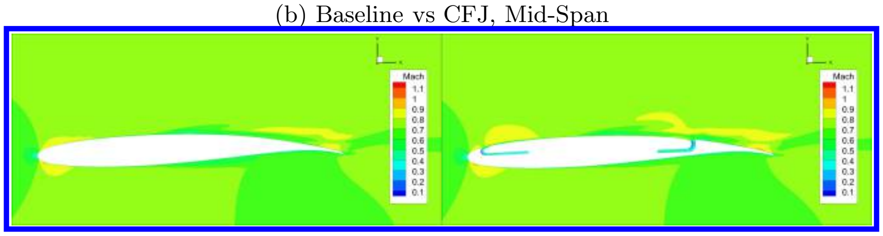

(c) Baseline vs CFJ, Tip

Figure 17: NASA SC(2)-1010 Mach Contours Baseline v CFJ. 10° Sweep, $\alpha = -3°$, $C_\mu = 0.002$, $AR = 10$, $M = 0.712$

III.D. RAE-2822 CFJ AR10 Wings

RAE-2822 is a transonic supercritical airfoil that is studied quite extensively. Liu et al.[1] showed that applying CoFlow Jet active flow control to the airfoil can enhance aerodynamic efficiency by 14.5%. Compared with NASA SC(2)-1010, the leading edge of RAE-2822 is sharper with a smaller radius. For this 3D transonic CFJ wing study, the previously optimized 2D RAE-2822 CFJ airfoil by Liu and Zha[1] with SST of 0.05% is used to form the 3D wing. The suction slot size, orientation and location are also kept the same as the 2D configuration. The injection slot size is 0.6%C located at 3% of chord. The suction location is 75% chord with the slot size of 1.2%C. The free stream conditions of M=0.729 and $Re = 6.5 \times 10^6$ are used. The objective of this RAE-2822 3D CFJ wing study is two fold: 1) Compare the 3D transonic CFJ wing using a 12% thickness supercritical airfoil with the wing of 10% thickness airfoil of NASA SC(2) 1010. 2) Investigate the CFJ transonic wing performance with a sharper leading edge shape of RAE-2822.

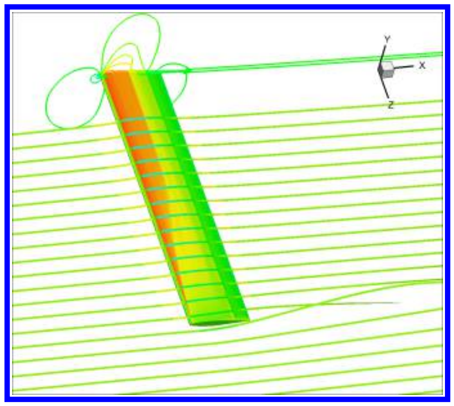

Figure 18: RAE-2822 AR10 CFJ Wing with Streamlines and Isentropic Mach Surface Contours

The first result is to compare the zero sweep baseline wing of aspect ratio 10 and the CFJ wing with a C_μ of 0.003, which is the optimal C_μ for the 2D airfoil.[1] The angle of attack is varied from 1.5° to 4° for cruise performance. As shown in Figure 19 the lift coefficient over the entire angle of attack range is higher for the CFJ wing than the baseline wing. The drag coefficient is also reduced with a very low CFJ power coefficient P_c. This contributes to a peak corrected aerodynamic efficiency for the CFJ wing at 2°, which is an improvement of 3% over the baseline wing at the AoA of 2.31° as shown in Figure 19. This is a fairly large reduction in efficiency improvement from the 2D case, which gains 14%. The CFJ wing peak productivity efficiency is increased by 12% compared with the baseline wing. To understand the decrease in efficiency improvement compared with the 2D case, it is important to examine the pressure and isentropic Mach distribution around the wing.

Figure 20 shows the isentropic Mach distribution at the root of the Baseline wing and 2D airfoil at an AoA of 2.31°. Noticeably the shock wave position is more upstream on the 3D wing compared to the 2D airfoil. The initial acceleration region is in the same location, but the value is somewhat mitigated for the 3D wing. The overall loading is smaller due to the effectively reduced AoA by downwash.

To more resemble the 2D loading, the AoA of the 3D wing is increased to 3deg and the isentropic Mach number is shown in Fig. 21. The baseline wing at the root does have the loading distribution closer to the 2D case for the suction peak, but the shock wave is still upstream of the 2D shock location and the shock strength is a little weaker. For the CFJ wing at C_μ of 0.003, the suction peak is substantially higher than the 2D case and the shock position is also upstream of the 2D and 3D baseline one, but the shock strength is also weaker than the 2D baseline airfoil and expect to generate smaller wave drag.

Figure 22 shows the root isentropic Mach number distribution of the baseline and CFJ wing when the angle of attack is further pushed to 3.5° to offset the downwash effect. The loading is definitely increased with the suction peak Mach number greater than that of the 2D baseline at AoA of 2.31°. Interestingly, the shock location is still at about the same location as at lower AoA. Unfortunately, the increase in shock strength, wave drag and induced drag hurt the overall performance of the CoFlow Jet wing at $\alpha = 3.5°$. The corrected aerodynamic efficiency is 3% lower than the baseline wing at the same angle of attack with a 7.6% increase in drag.

Figure 23 shows the isentropic Mach distribution at 90% span for the baseline and CFJ wings at an angle of attack of 3°. Also plotted is the distribution for the 2D baseline airfoil at AoA 2.31°. The outer

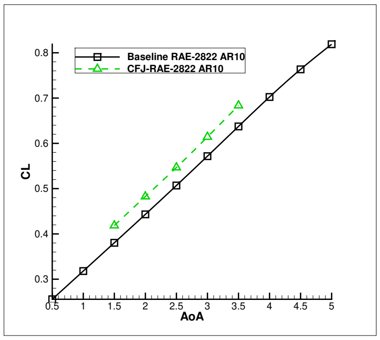

(a) C_L vs. AoA

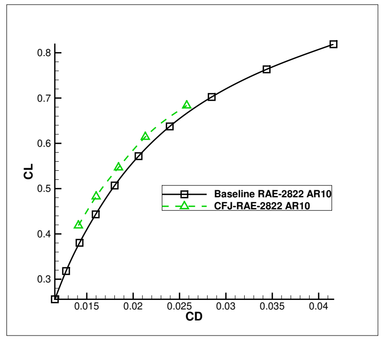

(b) C_L vs. C_D

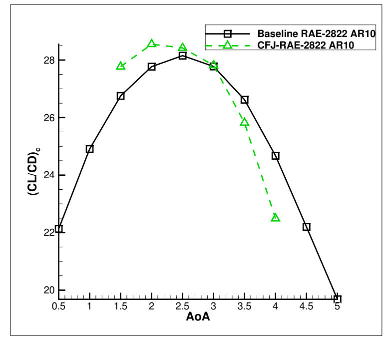

(c) $(C_L/C_D)_c$ vs. AoA

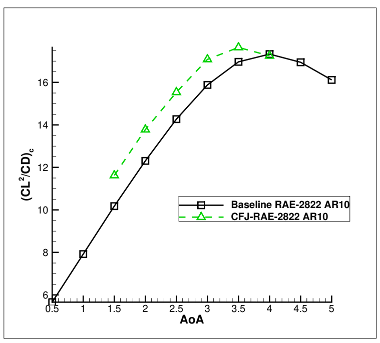

(d) $(C_L^2/C_D)_c$ vs. AoA

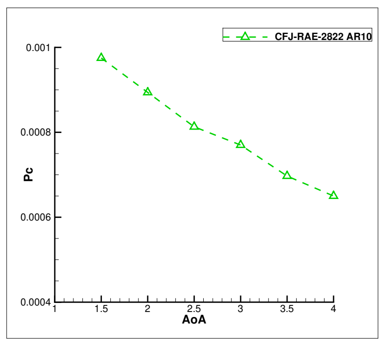

(e) P_c vs. AoA

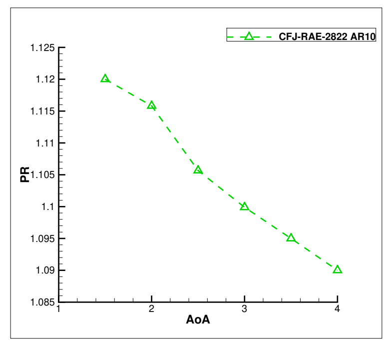

(f) Total Pressure Ratio vs. AoA

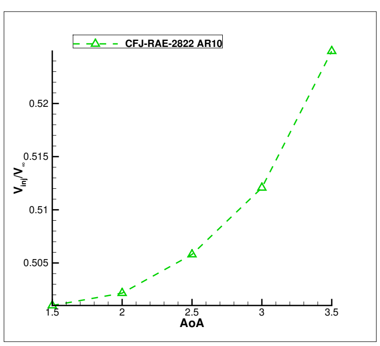

(g) Jet Velocity vs. AoA

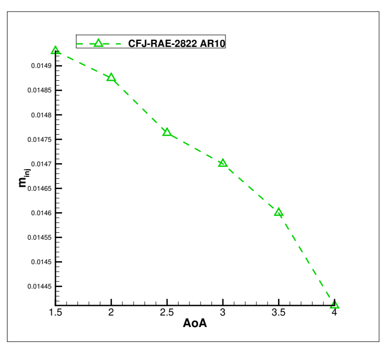

(h) Mass Flow-Rate vs. AoA

Figure 19: RAE-2822 Baseline v CFJ, $C_\mu = 0.003$, $AR = 10$, $M = 0.729$

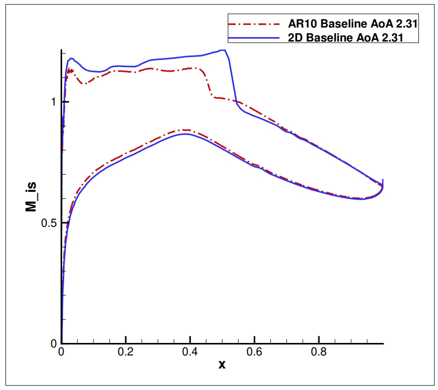

Figure 20: RAE-2822 AR10 Baseline Isentropic Mach Distribution, $\alpha = 2.31°$

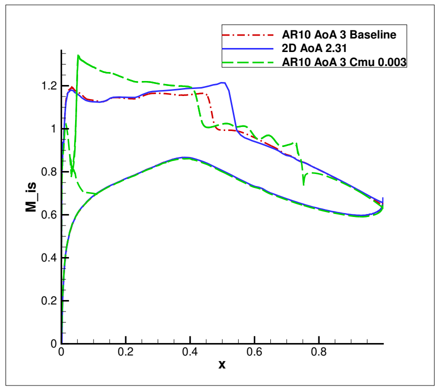

Figure 21: RAE-2822 AR10 Isentropic Mach Distribution, $\alpha = 3°$

span of the 3D baseline wing does not support a large supersonic region compared to the root of the wing because of the reduced tip loading due to tip vortex. This also affects the CFJ wing as it is not able to expand the supersonic region as at the inner span. As shown in Figure 23, the CFJ wing has a short supersonic spike, followed by a shock wave. The remainder of the distribution is about the same as that of the baseline wing except the spike at the suction slot.

III.D.1. Variable C_μ Along the Span

The study in the last section indicates that the CFJ with uniform strength (C_μ) along the span does not have much benefit near the tip region. It is because the load is reduced due to the tip vortex and the supersonic region is substantially reduced. This section hence will study the CFJ C_μ distribution varied along the span, in particular mitigated toward outer span to see if it improves the overall efficiency.

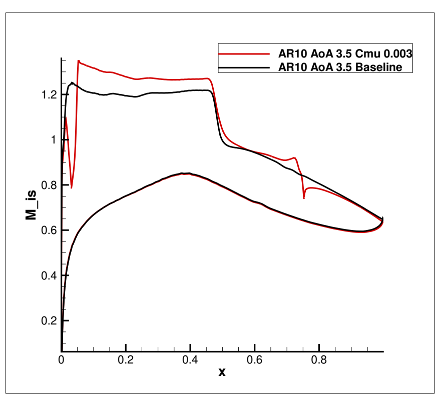

Figure 22: RAE-2822 AR10 Isentropic Mach Distribution, $\alpha = 3.5°$

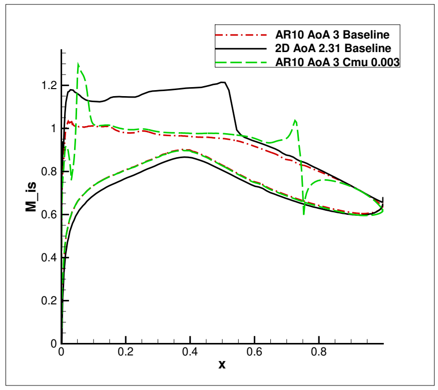

Figure 23: RAE-2822 AR10 Isentropic Mach Distribution, $\alpha = 3°$, 90% Span

The C_μ variation along span is achieved by varying the injection total pressure boundary condition to match the prescribed C_μ distribution at different spanwise segments. The single slot along the span is partitioned into 8 sub slots. Each spanwise segment injection slot has a prescribed C_μ. Varying the C_μ from root to tip "linearly" is actually a step function for each spanwise segment. The AoA is fixed at 3° because it resembles the 2D flow the most at the root area with a large supersonic region on the suction surface.

Table 5: CFJ-RAE-2822 $\alpha = 3°$, Variable C_μ, 100% Span

Case	C_μ **0%S**	C_μ **50%S**	C_μ **100%S**	C_L	C_D	P_c	C_L/C_D	$(C_L/C_D)_c$	C_L^2/C_{D_c}
Baseline	0	0	0	0.5712	0.0203	0.0000	28.15	28.15	16.08
CFJ-3D-1	0.003	0.003	0.003	0.6374	0.0234	0.0010	27.24	26.12	16.65
CFJ-3D-2	0.003	0.002	0.001	0.6322	0.0220	0.0006	28.73	27.97	17.68
CFJ-3D-3	0.003	0.0025	0.002	0.6357	0.0233	0.0010	27.23	26.14	16.62
CFJ-3D-4	0.003	0.004	0.005	0.6467	0.0235	0.0010	27.57	26.48	17.12
CFJ-3D-5	0.005	0.004	0.003	0.6483	0.0213	0.0025	30.50	27.27	17.68

Table 5 shows the results of linearly varying C_μ in the span-wise direction from the root of the wing to the tip. Case CFJ-3D-2 has a C_μ value of 0.003 at the root, which is decreased to 0.001 at the wing tip. CFJ-3D-3 has a slower decrease of C_μ with the value of 0.003 at the root to 0.002 at the wing tip. The CFJ-3D-3 case has a 0.6% higher lift coefficient due to the overall higher C_μ along the span, but also has a 6% higher drag coefficient due to the stronger shock wave and higher wave drag caused by the larger C_μ. The higher C_μ costs the CFJ-3D-3 case with a 67% greater CFJ power coefficient. This comparison indicates that reducing the CFJ momentum coefficient toward outer span is beneficial to wing system aerodynamic efficiency because the energy consumed to pump CFJ near the wing tip receives little benefit.

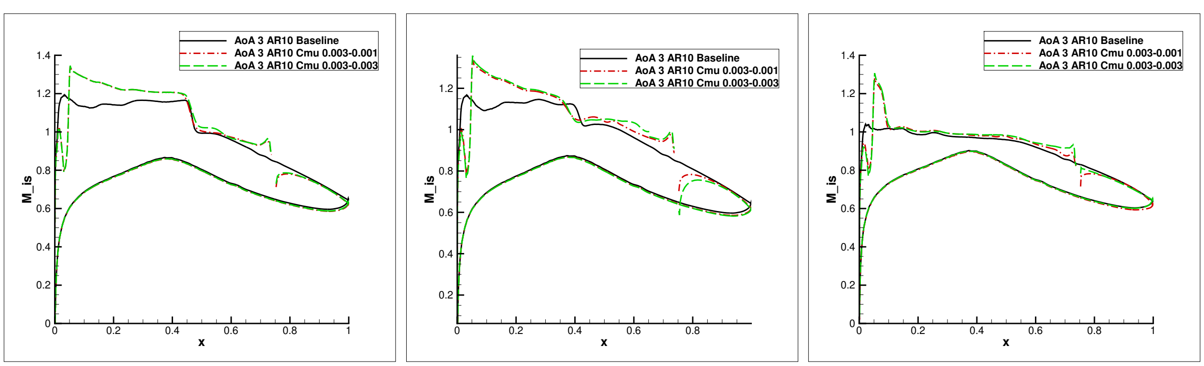

(a) Root, C_μ=0.003 (b) Mid-Span, C_μ=0.002 (c) 90% Span, C_μ=0.0012

Figure 24: CFJ-3D-2 Isentropic Mach Distribution vs Baseline at $\alpha = 3°$

Figure 24 shows the isentropic Mach distribution at different span-wise locations for the case CFJ-3D-2 compared with the baseline wing and CFJ-3D-1. At the root of each wing, the C_μ values are the same, 0.003. Their isentropic Mach number distributions are very similar with slightly higher Mach number before the shock than that of the baseline wing. At mid-span, the isentropic Mach number distribution for the case CFJ-3D-2 is actually more favorable with weaker shock than the baseline wing. At the wing tip, the CFJ generates a sharp spike at the injection and suction slot locations. This contributes little to enhance the lift coefficient, but increases the drag coefficient and CFJ power consumption.

It is useful to compare the two cases that have the same averaged jet strength, but distributed in an opposite way. Case CFJ-3D-4 has a C_μ distribution of 0.005 at the root and 0.003 at the tip, while case CFJ-3D-5 has a reversed C_μ distribution of 0.003 at the root and 0.005 at the tip. The average C_μ values in both cases is 0.004. These two cases show how much influence the tip region has for the CFJ wing performance compared to the root region. The mid-span region has the identical jet strength between the two cases. Both cases achieve about the same lift coefficients, but Case CFJ-3D-4, which has higher jet strength at the root, produces 10% less drag. It also has a much higher power coefficient, but the power coefficient is an order of magnitude smaller than the drag coefficient and has minimal impact on the aerodynamic efficiency comparison. The L/D_c value for CFJ-3D-5, is 3% higher than that of CFJ-3D-4 as shown in Table 5.

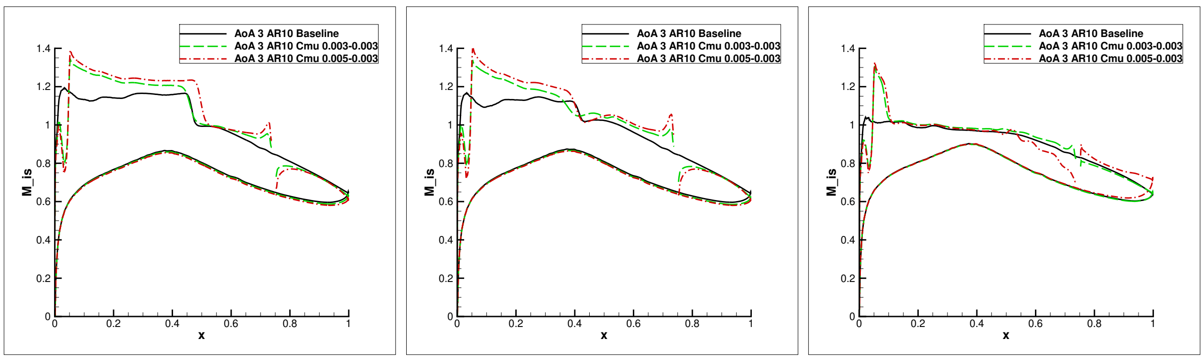

(a) Root, C_μ=0.005 (b) Mid-Span, C_μ=0.004 (c) 90% Span, C_μ=0.0032

Figure 25: CFJ-3D-4 Isentropic Mach Distribution vs Baseline at $\alpha = 3°$

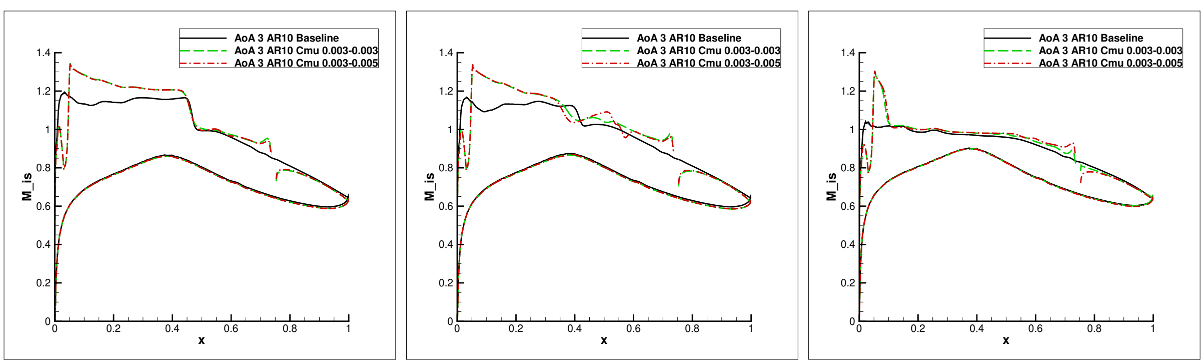

(a) Root, C_μ=0.003 (b) Mid-Span, C_μ=0.004 (c) 90% Span, C_μ=0.0048

Figure 26: CFJ-3D-5 Isentropic Mach Distribution vs Baseline at $\alpha = 3°$

Figures 25 and 26 show the isentropic Mach distribution at the root, mid-span and 90% span for CFJ-3D-4 and CFJ-3D-5 compared with CFJ-3D-1 that has a constant C_μ of 0.003. The CFJ strength of CFJ-3D-5 is higher at the root in Figure 25, which has the shockwave stronger, pushed more downstream and the loading increased. Both cases have the C_μ values of 0.004 mid-span. However, the high C_μ at the root also increases the loading at mid-span. Comparing both cases at 90% span is interesting. The overall loading difference is small using C_μ 0.005 or 0.003. Some differences lie in the flow momentum downstream toward the suction slot. Overall, having the jet strong at the root and weak at the tip is much more efficient than the opposite distribution.

III.D.2. Variable C_μ Along 90%, 70% and 50% Span

Since the tip region appears to be insensitive to CFJ flow control due to the shock wave and flow structures, this section conducts a study to keep 10% tip span the same as the original baseline RAE2822 airfoil with no CFJ. The purpose is to investigate if it improves the overall wing efficiency by saving the energy with CFJ applied for most of the inner span instead of the full span. These mesh changes are laid out in Figure 27 with the 10% tip span having no CFJ. The rest of the mesh is the same as the mesh used for the full span with CFJ. The CFJ injection and suction slots are still partitioned by 8 segments to locally control the jet strength.

The previous study shows an increase in aerodynamic efficiency over the baseline wing at an angle of attack of 3°. This section hence keeps the AoA at 3° to see the effect of no CFJ in the tip span. Two approaches are adopted in this study: 1) linear variation of C_μ along the span as in the previous section; 2) keep a constant C_μ for the inner 50% of the span, then linearly increase or decrease jet strength from 50% span to 90% span. Because the supersonic region starts to decrease significantly at 50% outer span as shown in Fig. 28, the second approach is chosen to see if it can be benefited more by varying the CFJ strength at the span from 50% to 90%.

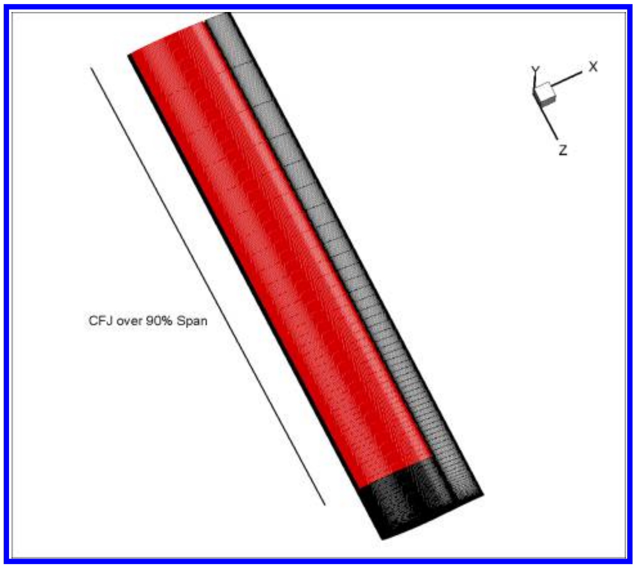

Figure 27: RAE-2822 AR10 Mesh, CFJ From 0% to 90% Span

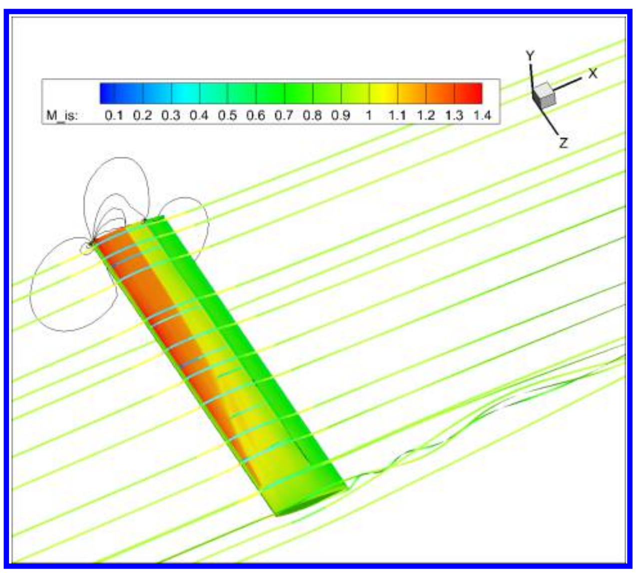

Figure 28: CFJ-3D-8 Surface Mach number contours with CFJ applied to 90% span

Table 6 shows the list of cases studied with the C_μ given at the root of 0% span (0%S), mid-span (50%S) and 90% span (90%S). The C_μ is varied linearly between two span locations. The lift coefficient is increased significantly for all the CFJ cases. It increases all the pure aerodynamic C_L/C_D since the drag is only slightly increased. The power coefficient remains one order of magnitude lower than the drag coefficient for all the cases. This results in the productivity efficiency increase for all the CFJ cases. Comparing the drag coefficient to the previous study with full span using CFJ, all the cases with 90% span have lower drag coefficients due to reduced tip loading while maintaining a high lift coefficient. The power coefficient is slightly increased, but remains very low. The decrease in drag increases the corrected aerodynamic efficiencies.

The two cases deserving particular attention are the cases CFJ-3D-7 and CFJ-3D-10, which gives the highest aerodynamic efficiency and productivity efficiency, respectively. Case CFJ-3D-7 linearly decreases jet strength from root to 90% span with C_μ varied from 0.005 to 0.001. This case enhances lift by 8%. The drag coefficient is basically the same as that of the baseline, much smaller that the 6% increase of the wing with full CFJ. This case has the productivity efficiency increased by 9%. For the case CFJ-3D-10, the C_μ is kept constant at 0.006 for the half span and is linearly reduced to 0.001 at 90% span. The higher C_μ increases the overall lift coefficient with higher power coefficient and slightly increased drag coefficient. The lift enhancement dominates the overall effect with the productivity efficiency of 11.7% higher than that of the baseline. The conclusion learned in this section is that for transonic wing, applying CFJ in the outer span is not effective to enhance lift due to the shrunk supersonic region. The energy consumption used by CFJ at the outer span outweighs the benefit.

Table 6: CFJ-RAE-2822 $\alpha = 3°$, Variable C_μ. CFJ Covering 90% Span

Case	C_μ **0%S**	C_μ **50%S**	C_μ **90%S**	C_L	C_D	**Pc**	**L/D**	**L/Dc**	C_L^2/C_{D_c}
Baseline	0	0	0	0.5712	0.0203	0.0000	28.15	28.15	16.08
CFJ-3D-6	0.005	0.004	0.003	0.6343	0.0210	0.0017	30.18	27.89	17.69
CFJ-3D-7	0.005	0.0025	0.001	0.6173	0.0204	0.0014	30.22	28.34	17.50
CFJ-3D-8	0.005	0.005	0.001	0.6314	0.0208	0.0016	30.33	28.13	17.76
CFJ-3D-9	0.003	0.003	0.001	0.6009	0.0207	0.0006	29.01	28.16	16.92
CFJ-3D-10	0.006	0.006	0.001	0.6424	0.0209	0.0021	30.78	27.97	17.97
CFJ-3D-11	0.003	0.003	0.003	0.6179	0.0210	0.0010	29.45	28.13	17.38
CFJ-3D-12	0.006	0.007	0.001	0.6498	0.0211	0.0026	30.84	27.51	17.88

A similar methodology was applied to keeping the outer 30% and 50% tip span the original baseline RAE2822 airfoil with no CFJ. Since the supersonic region decreases past 70% total span, measured from the root, there may be power savings by not applying CFJ to more of the outer span. This should also maintain most of the lift increase due to the CFJ since loading is greater at the wing root. It was seen in Table 6 in case CFJ-3D-9 that reducing C_μ in the outer span results in significant power savings. Table 7 shows the list of cases studied with CFJ applied to the inner 70% of the span. In order to decrease the variables studied, a constant C_μ as chosen along the entire CFJ. Case CFJ-3D-15 is similar to CFJ-3D-9 in that C_μ of 0.003 is used along most of the wing span. They both show similar performance with increased lift over baseline, and reduced power consumption. Lowering the C_μ to 0.002 in case CFJ-3D-14 results in a 1.2% increase in aerodynamic efficiency over baseline and a 5.7% improvement in lift coefficient. Productivity efficiency is similarly increased by 7.1%.

Table 7: CFJ-RAE-2822 $\alpha = 3°$, Constant C_μ. CFJ Covering 70% Span

Case	C_μ	C_L	C_D	**Pc**	**L/D**	**L/Dc**	C_L^2/C_{D_c}
Baseline	0	0.5712	0.0203	0.0000	28.15	28.15	16.08
CFJ-3D-14	0.002	0.6043	0.0208	0.0004	29.00	28.51	17.23
CFJ-3D-15	0.003	0.6091	0.0208	0.0008	29.37	28.26	17.21
CFJ-3D-16	0.004	0.6232	0.0209	0.0014	29.77	27.92	17.40

Reducing the CFJ to the inner 50% span was done to see whether any power savings are overpowered by a decrease in lift. As expected in Table 8, lift coefficients were lower than when the CFJ covered 70%

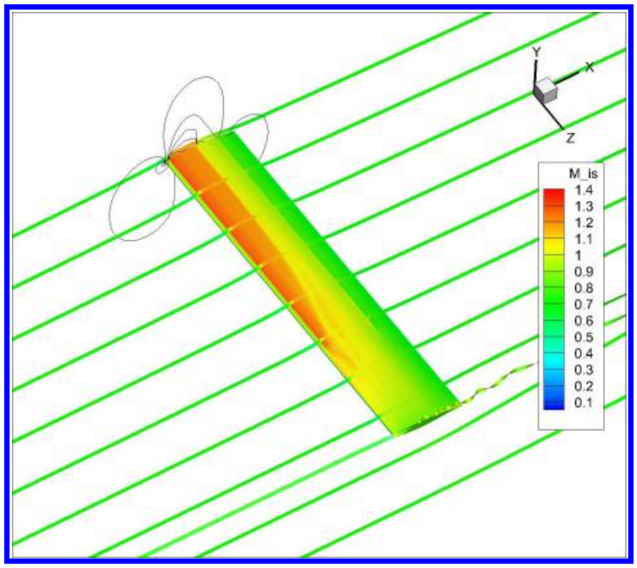

Figure 29: CFJ-3D-14 Surface Mach number contours with CFJ applied to 70% span

of the span. Power is reduced and does result in improved aerodynamic efficiency over baseline in case CFJ-3D-17. The overall performance is lower than case CF-3D-14 as C_L/C_{D_c} and productivity efficiency takes a hit due to less lift improvement. The isentropic Mach surface contours seen in Figures 29 and 30 portray cases CFJ-3D-14 and CFJ-3D-17, respectively. The inner span where CFJ is active has a consistent supersonic region. The difference between 50% and 70% CFJ span show that the CFJ wing can support a strong supersonic region up to 70% span.

Table 8: CFJ-RAE-2822 $\alpha = 3°$, Constant C_μ. CFJ Covering 50% Span

Case	C_μ	C_L	C_D	**Pc**	**L/D**	**L/Dc**	C_L^2/C_{D_c}
Baseline	0	0.5712	0.0203	0.0000	28.15	28.15	16.08
CFJ-3D-17	0.002	0.5878	0.0205	0.0003	28.74	28.35	16.67
CFJ-3D-18	0.003	0.6000	0.0208	0.0005	28.84	28.13	16.88
CFJ-3D-19	0.004	0.6082	0.0210	0.0009	29.00	27.78	16.90

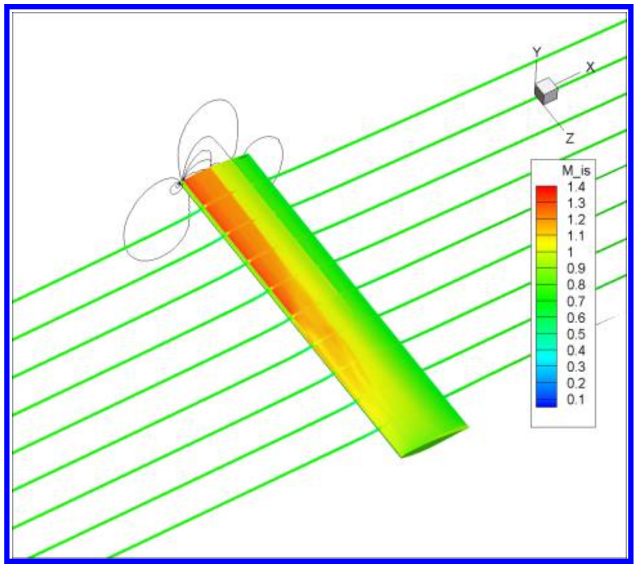

Figure 30: CFJ-3D-17 Surface Mach number contours with CFJ applied to 50% span

IV. Conclusion

For the 3D wing formed by the NASA SC(2)-1010 supercritical airfoil with aspect ratio of 10, the wing with no sweep achieves an improvement for C_L/C_{Dc} by 10% and C_L by 10% at the same time. Smaller gains of 6% is obtained for the same wing with a 10° sweep angle. The reason that the swept wing efficiency improvement is less than the non-swept wing is considered due to the misalignment of the CFJ with the main flow. Future work should be done to better align the CFJ with the mainflow. For the transonic wing formed by RAE2822 airfoil with aspect ratio of 10, applying CFJ in the outer span is not effective to enhance lift due to the shrunk supersonic region. The energy consumption used by CFJ at the outer span outweighs the benefit. For a design with CFJ applied from root to 90%, the productivity efficiency is significantly increased by 11%. Reducing the size of the CFJ region to 70% has the corrected aerodynamic efficiency improved by 1.2% over the baseline wing in case CFJ-3D-14. This happens while lift increases by 5.7% percent. Further applying CFJ to the inner 50% span shows the power reduction benefit, while still increasing lift and aerodynamic efficiency, but at a smaller amount. The cases with CFJ covering 70% span seem to best balance an improvement in lift and aerodynamic efficiency over the baseline wing.

V. Acknowledgments

The simulations are conducted on Pegasus supercomputing system at the Center for Computational Sciences at the University of Miami.

Disclosure: The University of Miami and Dr. Gecheng Zha may receive royalties for future commercialization of the intellectual property used in this study. The University of Miami is also equity owner in CoFlow Jet, LLC, licensee of the intellectual property used in this study.

References

[1] Liu, Z.-X. and Zha, G.-C. Transonic Airfoil Performance Enhancement Using Co-Flow Jet Active Flow Control. AIAA Paper 2016-3472, AIAA AVIATION 2016, 8th AIAA Flow Control Conference, Washington, D.C, June 13-17, 2016.

[2] Boling, J. and Dhakaly, S. and Yang, Y.-C. and Zha, G.-C. Numerical Investigation of Low Speed Performance of Transonic CoFlow Jet Supercritical Airfoil. AIAA Paper 2017-3249, AIAA AVIATION Forum, 35th AIAA Applied Aerodynamics Conference, 5-9 June 2017, Denver, Colorado, 15-19 June, 2020.

[3] G.-C. Zha and D. C. Paxton. A Novel Flow Control Method for Airfoil Performance Enhancement Using Co-Flow Jet. *Applications of Circulation Control Technologies*, Chapter 10, p. 293-314, Vol. 214, Progress in Astronautics and Aeronautics, AIAA Book Series, Editors: Joslin, R. D. and Jones, G.S., 2006.

[4] G.-C Zha and C. Paxton and A. Conley and A. Wells and B. Carroll. Effect of Injection Slot Size on High Performance Co-Flow Jet Airfoil. *AIAA Journal*, 43, 2006.

[5] G.-C. Zha and W. Gao and C. Paxton. Jet Effects on Co-Flow Jet Airfoil Performance. *AIAA Journal, No. 6*, 45:1222–1231, 2007.

[6] G.-C Zha and B. Carroll and C. Paxton and A. Conley and A. Wells. High Performance Airfoil with Co-Flow Jet Flow Control. *AIAA Journal*, 45, 2007.

[7] Wang, B.-Y. and Haddoukessouni, B. and Levy, J. and Zha, G.-C. Numerical Investigations of Injection Slot Size Effect on the Performance of Co-Flow Jet Airfoil . *AIAA Journal of Aircraft*, 45:2084–2091, 2008.

[8] B. P. E. Dano, D. Kirk, and G.-C. Zha. Experimental Investigation of Jet Mixing Mechanism of Co-Flow Jet Airfoil. AIAA Paper 2010-4421, 5th AIAA Flow Control Conference, Chicago, IL,, 28 Jun - 1 Jul 2010.

[9] B. P. E. Dano, G.-C. Zha, and M. Castillo. Experimental Study of Co-Flow Jet Airfoil Performance Enhancement Using Micro Discreet Jets. AIAA Paper 2011-0941, 49th AIAA Aerospace Sciences Meeting, Orlando, FL,, 4-7 January 2011.

[10] Lefebvre, A. and Dano, B. and Di Franzo, M. and Bartow, W. and Zha, G.-C. Performance of Co-Flow Jet Flow Airfoil with Variation of Mach Number. AIAA Paper 2013-0490, 51st AIAA Aerospace Science Meeting, Grapevine, TX, 7-10 Jan. 2013, to appear in Journal of Aircraft, 2016.

[11] Lefebvre, A. and Zha, G.-C. Numerical Simulation of Pitching Airfoil Performance Enhancement Using Co-Flow Jet Flow Control. AIAA Paper 2013-2517, 31st AIAA Applied Aerodynamics Conference, San Diego, CA, 24 - 27 June 2013.

[12] Lefebvre, A. and Zha, G.-C. . Design of High Wing Loading Compact Electric Airplane Utilizing Co-Flow Jet Flow Control. AIAA Paper 2015-0772, AIAA SciTech2015: 53nd Aerospace Sciences Meeting, Kissimmee, FL, 5-9 Jan 2015.

[13] Lefebvre, A. and Dano, B. and Bartow, W. and Di Franzo, M. and Zha, G.-C. Performance and Energy Expenditure of Co-Flow Jet Airfoil with Variation of Mach Number. *AIAA Journal of Aircraft*, 53:1757–1767, 2016.

[14] Yang, Y.-C. and Zha, G.-C. Super-Lift Coefficient of Active Flow Control Airfoil: What Is the Limit? AIAA Paper 2017-1693, AIAA SCITECH2017, 55th AIAA Aerospace Science Meeting, Grapevine, Texas, 9-13 January 2017.

[15] G.-C. Zha, Y. Yang, Y. Ren, and B. McBreen. Super-Lift and Thrusting Airfoil of Coflow Jet Actuated by Micro-Compressors . AIAA Paper-2018-3061, AIAA AVIATION Forum 2018, 2018 Flow Control Conference, Atlanta, Georgia, June 25-29, 2018.

[16] G.-C. Zha, Y. Shen, and B. Wang. An improved low diffusion E-CUSP upwind scheme . *Journal of Computer & Fluids*, 48:214–220, 2011.

[17] B.-Y. Wang and G.-C. Zha. A General Sub-Domain Boundary Mapping Procedure For Structured Grid CFD Parallel Computation. *AIAA Journal of Aerospace Computing, Information, and Communication*, 5, No.11:2084–2091, 2008.

[18] Y.-Q. Shen, G.-C. Zha. Improvement of weighted essentially non-oscillatory schemes near discontinuity. AIAA paper 2009-3655, 2009.

[19] K.-W. Xu and G.-C. Zha. High control authority 3d aircraft control surfaces using co-flow jet. *AIAA Journal of Aircraft*, July 2020.